

Rapid forecast of tsunami wave heights from a database of pre-computed simulations, and application during the 2011 Tohoku tsunami in French Polynesia

D. Reymond,¹ E. A. Okal,² H. Hébert,³ and M. Bourdet⁴

Received 14 March 2012; revised 17 April 2012; accepted 19 April 2012; published 5 June 2012.

[1] We present a method for the rapid estimation of tsunami wave heights, either in the deep Pacific Basin, or at specific shore locations. It uses a database of 260 pre-computed scenarios of generic sources distributed along the Pacific trenches, and can provide an estimate of wave heights within minutes of the location of the earthquake and the estimation of its moment. The method is tested against a set of DART data, and of 51 maregraph records in Tahiti and the Marquesas Islands. It was used in real time to successfully predict tsunami amplitudes in Polynesia during the 2011 Tohoku alert. **Citation:** Reymond, D., E. A. Okal, H. Hébert, and M. Bourdet (2012), Rapid forecast of tsunami wave heights from a database of pre-computed simulations, and application during the 2011 Tohoku tsunami in French Polynesia, *Geophys. Res. Lett.*, 39, L11603, doi:10.1029/2012GL051640.

1. Introduction

[2] Numerical simulations constitute the most efficient tool for estimating tsunami propagation and forecasting the distribution of their amplitudes both on the high seas and at shorelines. Assuming the availability of a model of the seismic source, and of adequate bathymetry, waveform simulations have now reached an impressive, occasionally spectacular, level of accuracy [e.g., Hébert *et al.*, 2009a, Figure 11; Tang *et al.*, 2010, Figure 9]. Even though computing capabilities are constantly improving, the main obstacle for the routine use of numerical simulations for tsunami warning under real-time operational conditions remains the slowness of the numerical computation, which is aggravated when fine grids are required for the precise modeling of the coastline response on the scale of an individual harbor. For example, the full scale modeling of a tsunami propagating for 15 hours over the Pacific Basin, followed by its interaction with 10 sites on 5 islands, would take about one day of computation on a single processor.

In simple terms, the computation proceeds slower than the tsunami across the ocean, which is clearly unacceptable in the framework of real-time warning.

[3] In this context, an alternative strategy consists of pre-computing simulations for a large number of scenarios, thus building a catalogue which can be looked up and fine-tuned as soon as an adequate estimate of the seismic source becomes available. Such an algorithm (SIFT) was developed by Titov *et al.* [2005] and has been implemented at the US Tsunami Warning Centers. Their method uses rapid estimates of epicenter and moment to expand the parent earthquake onto a grid of unitary seismic sources, whose pre-computed simulations are then weighted and combined to produce a tsunami forecast in the far field.

[4] In this paper, we present an alternative, fast forecasting method based on the selection of a pre-computed series of tsunami scenarios. As will be detailed below, for each epicentral region with tsunamigenic potential in the Pacific Basin, we pre-compute several scenarios of seismic source, covering three orders of magnitude in seismic moment, whose wave height fields in the far field are permanently catalogued. We discuss the operational application of this algorithm to the case of the great Tohoku tsunami of 11 March 2011.

[5] Our approach differs from Titov *et al.*'s [2005], in that it uses a catalogue of pre-computed forecasts spanning a large range of source sizes (including mega-shocks comparable to the 2011 Tohoku event), thus limiting the inter- or extrapolation to less than one order of magnitude. As such, it minimizes the effects of possible non-linearities when building a potentially gigantic source from a very large number of elementary solutions. We present it as a rapid, “quick-and-dirty” alternative to the more elaborate SIFT algorithm.

2. The Database of 260 Pre-computed Tsunami Scenarios

2.1. Numerical Simulations

[6] We follow the standard approach to tsunami simulation, in which the static displacement of the ocean floor created by the seismic dislocation is transposed to the sea surface and used as an initial condition of the system of partial differential equations expressing the evolution of the wavefield under the laws of hydrodynamics. This approximation is justified by the fact that all seismic ruptures, including exceptionally slow ones characteristic of the so-called “tsunami earthquakes”, remain hypersonic with respect to tsunami propagation. We use the non-linear shallow-water approximation to the Navier–Stokes equations expressing the conservation of mass

¹Laboratoire de Géophysique de Pamatai, CEA, DAM, DASE, Papeete, French Polynesia.

²Department of Earth and Planetary Sciences, Northwestern University, Evanston, Illinois, USA.

³CEA, DAM, DIF, Arpajon, France.

⁴Fugro Seismic Imaging AS, Oslo, Norway.

Corresponding author: D. Reymond, Laboratoire de Géophysique de Pamatai, CEA, DAM, DASE, PO Box 640, Papeete, Tahiti, 98713 French Polynesia. (reymond.d@labogeo.pf)

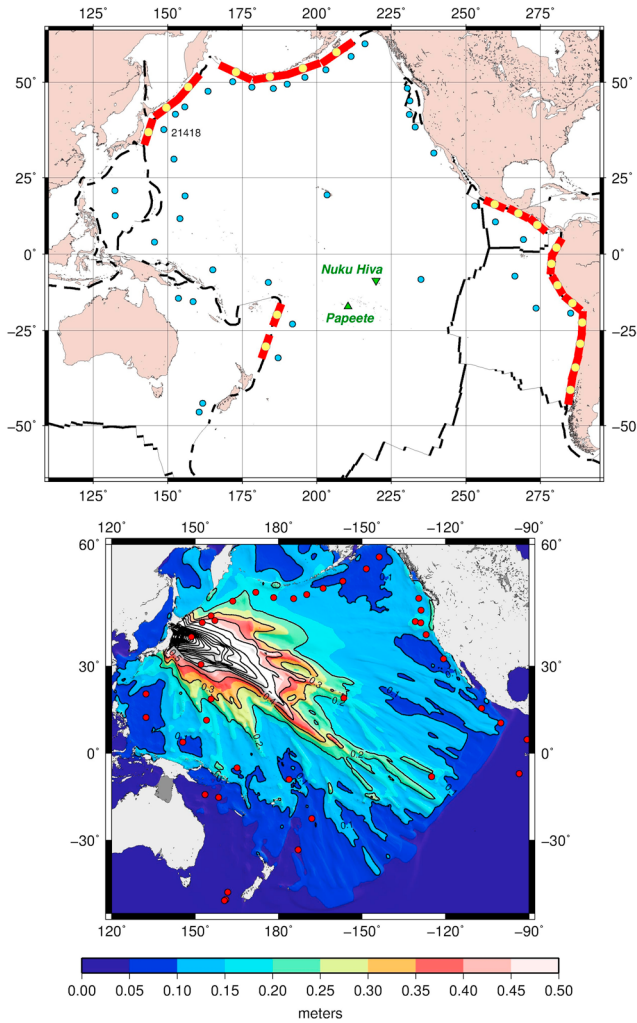


Figure 1. (top) Map of the Pacific Basin showing the rupture segments of the 20 MEGA sources (with the relevant centroids shown as open circles). The solid dots are the locations of the DART sensors. The triangles locate the harbors of Papeete, Tahiti and Taiohae, Nuku Hiva (Marquesas). (bottom) Field of MAX values obtained at the final time step ($t = 15$ h) for the simulation of the 2011 Tohoku tsunami. The reds dots are the locations of the DART sensors.

and momentum averaged over the thickness h of the oceanic column:

$$\frac{\partial(\eta + h)}{\partial t} + \nabla \cdot [\mathbf{v}(\eta + h)] = 0 \quad (1)$$

$$\frac{\partial \mathbf{v}}{\partial t} + (\mathbf{v} \cdot \nabla) \mathbf{v} = -g \nabla \eta \quad (2)$$

where η is the vertical displacement of the sea surface, \mathbf{v} the depth-averaged horizontal particle velocity, g the acceleration of gravity. These equations are then solved iteratively by a finite difference scheme [Hébert *et al.*, 2001].

2.2. Source Modelling

[7] Given a model of elastic dislocation, the coseismic displacement (CSD) of the ocean floor is computed using

Okada's [1985] formulae. We recall that, in addition to the epicentral location of the source, this computation requires eight parameters, namely centroid depth H , focal geometry (ϕ , δ , λ), fault dimensions L , W , fault slip D , and Poisson ratio ν (which in practice will be taken as $1/4$).

2.3. Source Locations and Sizes

[8] We place sources in 20 regions identified as posing a tsunami threat to French Polynesia. For each region, and following Hébert *et al.* [2009b], we envision three levels of seismic moments, namely 10^{21} , 10^{22} and 10^{23} N*m, which will be referred to as "AVERAGE", "BIG", and "MEGA". We place one MEGA event in each region (Figure 1, top), as a worst case scenario, even though that region may not have experienced a comparable earthquake during its recorded history. In the context of the scaling laws discussed below, we place four BIG sources and eight AVERAGE ones (displaced laterally) in each region, for a grand total of 260 sources.

2.4. Scaling Laws and Fault Parameters

[9] For each source size, we derive fault dimensions L , W , D using scaling laws [Kanamori and Anderson, 1975; Geller, 1976], which assume a constant rigidity $\mu = 510^{10}$ N/m² and a constant aspect ratio ($W = L/2$). For the MEGA sources, and following Scholz [1982], we use a thinner source ($W = L/4$). All resulting fault parameters are listed in Table S1 in the auxiliary material.¹

2.5. Source Geometry

[10] In an operational context, there is generally no time to obtain a precise focal geometry of the seismic source. We thus build our reference models under the assumption of a pure thrust mechanism expressing interplate slip at the subduction interface.

[11] This rather crude assumption is shared with Titov *et al.*'s [2005] algorithm and is justified by the fact that the overwhelming majority of damaging tsunamis are generated by large interplate thrust events. It is however not without exceptions, the most significant ones being normal faulting outer rise events, such the 1933 Sanriku earthquake whose tsunami was damaging in the far field, or complex composite mechanisms such as the 2009 Samoa earthquake. Incidentally, adequate estimates of wave heights were obtained for the latter event despite the use of an inaccurate mechanism [Okal *et al.*, 2010].

[12] In this context, the fault strike ϕ can be estimated reliably from the azimuth of the trench, as expressed in the bathymetry. For each subduction zone, the dip δ is chosen by averaging its values for all relevant CMT solutions with magnitude >6.5 . Finally, the slip angle λ was fixed at 90° ; this may become inaccurate in the case of significantly oblique subduction, but was chosen to maximize the vertical component of CSD.

2.6. Source Depth

[13] In a real-time operational environment, this parameter is also generally poorly resolved. We follow Okal [1988] who showed that far-field tsunami excitation depends only weakly on source depth for $h < 70$ km, and run our

¹Auxiliary materials are available in the HTML. doi:10.1029/2012GL051640.

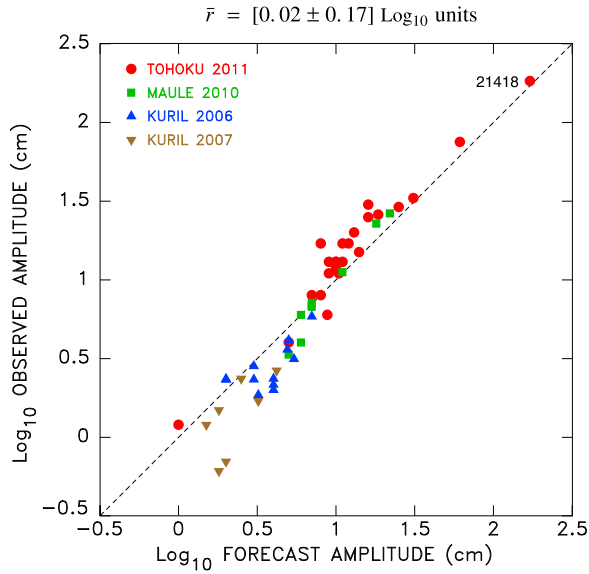


Figure 2. Observed versus forecast wave heights at DART sensors for the four recent large Pacific tsunamis. Note that our algorithm correctly predicts even the exceptionally high amplitude of 1.8 m for the Tohoku tsunami at the nearby site 21418.

simulations for a centroid depth of 35 km, which we found empirically to maximize far-field tsunami excitation.

2.7. Product Catalogue

[14] For each scenario, the simulations are run in the Pacific Basin for a propagation time of 15 hours, sufficient to include the arrival of the tsunami in Polynesia from all the regions considered, using a grid sampling of 10 arcmin, and a time step $\delta\tau = 10$ s, satisfying the stability condition of *Courant et al.* [1928]. The full time series of the wave heights at the locations of the 37 DART sensors deployed as of 2009 (see Figure 1, top) are permanently archived into a database of 9260 waveforms sampled at $\delta\tau = 10$ s. In addition, the maximum elevation reached at a given location is updated every hour at all points of the grid to define a running maximum amplitude $MAX(x, y; t)$

$$MAX(x, y; t) = \max_{\tau \leq t} [\eta(x, y, \tau)] \quad (3)$$

where the time sampling is one hour on t and $\delta\tau = 10$ s on τ . The fields MAX (totalling 3900) are then permanently archived.

2.8. Scaling With Moment

[15] Since only 3 levels of moment are simulated, the catalogued results must be adjusted to the exact moment value of any individual earthquake. For events between 10^{21} and 10^{23} N.m, a simple linear interpolation is performed. This represents the overwhelming majority of earthquakes with a potentially damaging tsunami in the far field. For other events, we extrapolate the AVERAGE and MEGA simulations, below 10^{21} and above 10^{23} N*m, respectively, using the spline function

$$\log_{10}\eta = -2.71 + 0.90(\log_{10}M_0 - 20) - 0.06(\log_{10}M_0 - 20)^2 \quad (4)$$

derived from a quadratic regression of an enhanced dataset of transpacific simulations [Hébert et al., 2009b]. Note that for events smaller than AVERAGE, this correction is essentially linear, while for the exceptional events, larger than MEGA, it grows slower than linearly, reflecting the narrowing with increasing moment, of the lobe of directivity due to source finiteness [Ben-Menahem and Rosenman, 1972; Talandier and Okal, 1991]. Figure 1 (bottom) gives an example of the field MAX in the case of the 2011 Tohoku tsunami for the final time step $t = 15$ h.

3. Validation Test: Comparison With Observed DART Data

[16] In Figure 2, we compare amplitudes forecast by our algorithm with those actually recorded on DART sensors for four large Pacific Basin tsunamis: the Kuril Islands doublet of 2006 and 2007, and the 2010 Maule, Chile, and 2011 Tohoku events. We find an excellent agreement, with an average residual $\bar{r} = -0.02 \pm 0.17$ logarithmic units for the full dataset of 51 points. The only scatter occurs for very small amplitudes (forecast or observed < 3 cm); in addition the generally deficient values observed for the 2007 Kuril normal faulting earthquake may illustrate the inadequate focal mechanism used in the forecast, as well as a violation of scaling laws by this event featuring a high stress drop.

4. From the High Seas to the Shore Line: Validation From Maregraph Records

[17] When faced with the problem of the interaction of the tsunami wavefield with a shoreline, any numerical simulation must be performed over an increasingly fine grid, which in turn mandates a reduced time step, and the use of a fully non-linear code. In an operational context, such calculations become prohibitively time-consuming. Consequently, we opt for a simple, computationally very fast, method, which provides surprisingly good estimates of the inundation inside individual harbors. We start by using *Green's* [1838] law

$$\frac{\eta_2}{\eta_1} = \left(\frac{h_1}{h_2}\right)^{\frac{1}{4}} \quad (5)$$

expressing conservation of wave energy flux, to prolong the gridded wave field into the harbor at depth h_2 , with respect to a nearby deep-water grid point at depth h_1 . This constitutes a drastic approximation, which is admittedly difficult to justify; we note however that *Hayashi* [2010] have successfully tested this approach to simulate the 1896 Meiji Sanriku tsunami. Of course, the complex response of a particular harbor does not follow Green's law exactly, but we found that it can be approached using an empirical correction factor β such that

$$\frac{\eta_2}{\eta_1} = \left[1 + \beta \frac{(H_E - h_2)}{H_E}\right] \cdot \left(\frac{h_1}{h_2}\right)^{\frac{1}{4}} \quad (6)$$

This expression provides a linear approximation of the response between the depth h_E at the entrance of the harbor (which we take as 50 m), and the target point. In the case of Papeete harbor, we use $\beta = -0.35$, a negative value expressing the attenuating role of the coral reef surrounding Tahiti. In the case of Taiohae (Nuku Hiva, Marquesas), we

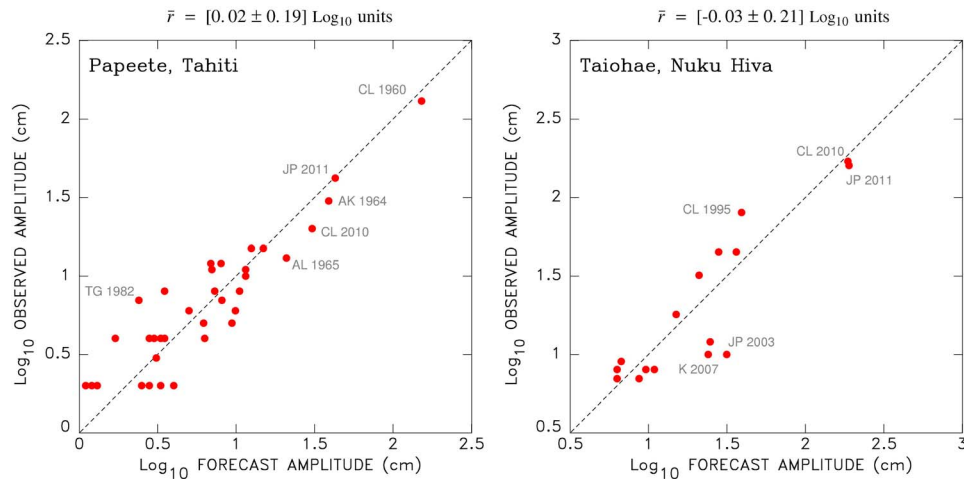


Figure 3. (left) Zero-to-crest amplitudes observed for 35 tsunamis on the Papeete, Tahiti maregraph versus forecasts obtained from equation (6). (right) Same as Figure 3 (left) but for 16 tsunamis recorded at Taiohae, Marquesas, since the deployment of the instrument in 1995.

use $\beta = 1.10$, this positive value expressing the enhanced response of this particularly narrow bay.

[18] We then proceed to compute forecast values at the local maregraphs, using $h_1 = 4000$ m, $h_2 = 20$ m in Papeete and 6 m in Taiohae. Figure 3 presents a comparison with values observed on the Papeete maregraph for 35 tsunamis in the past 53 years (data predating 1969 were recorded at other sites on Tahiti island and corrected to reflect differences in site responses). The average logarithmic residual, $\bar{r} = 0.02 \pm 0.19$, remains small, and again most of the scatter occurs for the smaller sources. Note in particular that the largest tsunamis (1960 and 2011) are perfectly well predicted, while other large events (1964, 2010, 1965) have a tendency to be slightly overpredicted by our forecast. On the other hand, the most underpredicted tsunami ($r = 0.47$) is from the smaller 1982 Tonga event, characterized as a slow “tsunami earthquake” [Newman and Okal, 1998], whose published CMT moment may underestimate the static value. An example of the distribution of tsunami heights forecast for 2011 in Papeete harbor is given by Figure 4 (left). It shows an average wave height of 40 to 52 cm in the harbor, where the maregraph recorded a maximum amplitude of 42 cm. A preliminary version of this map was obtained in real time during the alert, approximately 75 mn after origin time, i.e., 10 hours before the arrival of the waves in Polynesia [Reymond et al., 2012].

[19] Similar conclusions ($\bar{r} = -0.03 \pm 0.21$) are reached for the dataset of 16 tsunamis recorded at Taiohae since the maregraph was deployed in 1995 (Figure 3). Note that the two recent large tsunamis (Maule 2010 and Tohoku 2011) are very well predicted. The most overestimated events are the 2003 Hokkaido earthquake ($r = -0.50$), whose source was largely under land, and the “snappy” 2007 Kuril event ($r = -0.38$). Conversely, the most underestimated datum ($r = 0.31$) is the 1995 Chilean event, for the which the CMT solution underestimates the static moment [Pritchard et al., 2002].

4.1. The Case of the “Tsunami-Earthquakes”

[20] These events, defined by Kanamori [1972] as generating tsunamis greater than expected from their seismic

magnitudes (especially conventional ones), remain a major challenge in the context of tsunami warning. Models of their generation have often (but not always) invoked rupture in weak “sedimentary” material, either along the plate interface [Bilek and Lay, 1999] or in the overriding wedge [Fukao, 1979]. Okal [1988] has shown theoretically that rupture in sedimentary material leads to an enhanced ratio of tsunami to mantle wave excitation.

[21] In this context, tsunami earthquakes are clear violators of seismic scaling laws and would be expected to give rise to tsunamis of greater amplitude than derived using pre-computed simulations, which are based on scaling laws. Unfortunately, no such events have occurred in the Pacific Basin since 1996 (Chimbote, Peru), where they predate the deployment of the DART sensor network, so that a systematic test of this conjecture is impossible. We note however that tsunami earthquakes, which can feature rupture velocities as slow as 1 km/s, are characterized by source slowness, expressed for example through a deficient energy-to-moment ratio [Newman and Okal, 1998]. In this respect, they can be regarded as the exact opposite of the “snappy” intraplate earthquakes featuring higher than normal stress drops and E/M_0 ratios, such as the 2007 Kuril event. The latter was overpredicted both at DART stations and at Taiohae (see above), suggesting that, conversely, tsunami earthquakes should be underpredicted. This suggestion is supported by the case of the 1982 Tonga event, which has been recognized as a tsunami earthquake [Newman and Okal, 1998; Okal et al., 2003], and features the largest residual ($r = 0.47$) in the Papeete maregraph dataset. Observations of underpredicted forecast amplitudes could, in principle, add an additional component to the real-time identification of tsunami earthquakes.

4.2. The 2011 Japanese Tsunami in Nuku Hiva

[22] Finally, Figure 4 (right) presents a map, again obtained in real time, of the wave heights forecast in Taiohae Bay for the 2011 Tohoku tsunami, using equation (6). The predicted amplitudes at the Northwestern shore (2.0 m) is somewhat less than surveyed (2.55 and 2.70 m; hexagons on Figure 4, right), while the amplitude predicted at the

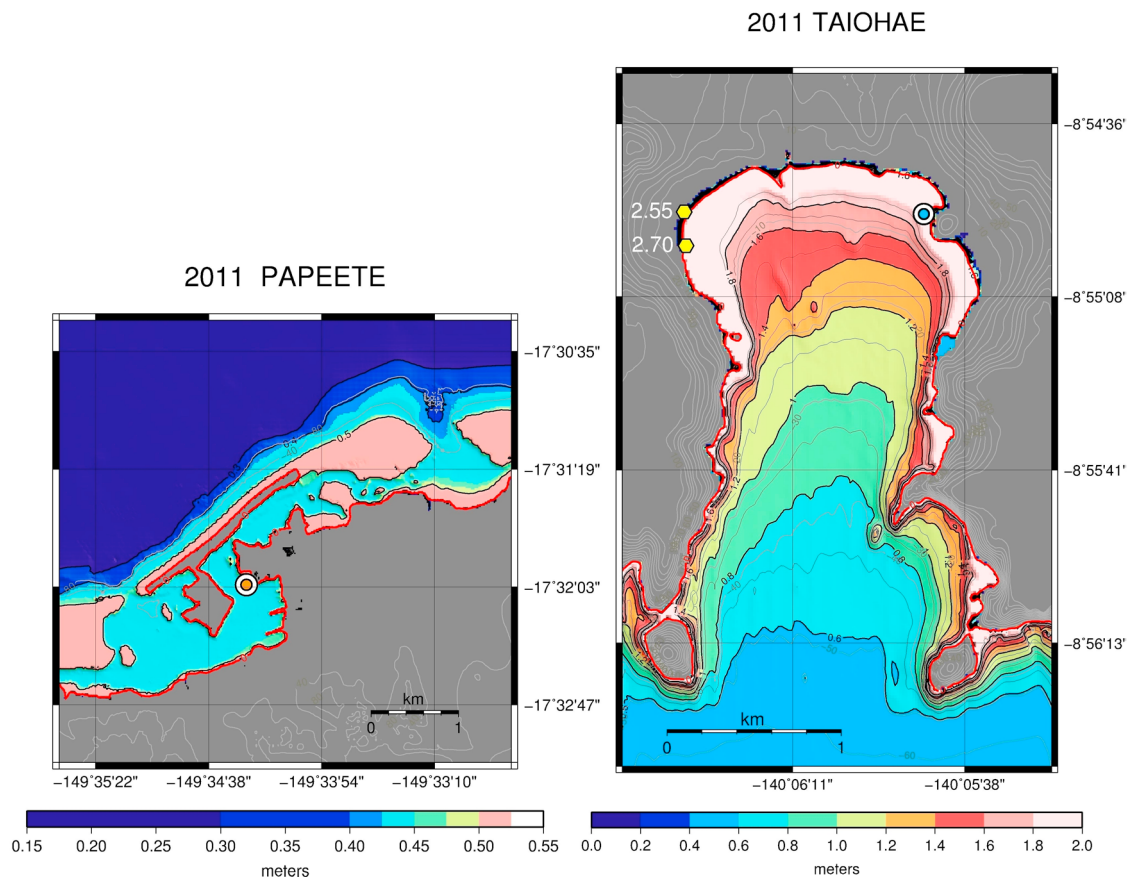


Figure 4. (left) Tsunami heights forecast inside Papeete harbor for the 2011 Tohoku event using equation (6). The majority of the harbor is forecast at an amplitude of 0.40 to 0.52 m. For reference, the maregraph, shown as the bull’s eye symbol, recorded a maximum (zero-to-crest) of 0.42 m. (right) Tsunami heights forecast at Taiohae harbor, Nuku Hiva for the 2011 Tohoku event, using equation (6). Note that the maximum surveyed run-up (2.55 and 2.70 m; hexagons) are larger than forecast (2.0 m) in the Northwestern part of the bay, whereas the amplitude recorded at the maregraph (1.6 m; bull’s eye symbol) is slightly overpredicted.

maregraph location (1.89 m; bull’s eye symbol) is slightly larger than actually recorded (1.60 m). This disparity of performance of the forecast on the two sites of the bay is an illustration of the limitation of Green’s law to the case of a strongly indented bay with an irregular bathymetry, the NW side shoaling more smoothly than the abrupt NE side. In particular, this is in contrast to the case of Papeete (Figure 4, left), where the bathymetry of the harbor is both shallower and more regular.

[23] At any rate, and from the standpoint of formulating an evacuation, it would be illusory to pretend to give an accurate forecast of the variations of wave heights on a scale of 1 km within strongly indented bays such as that of Taiohae. Rather, we show here that our approach can more realistically estimate the average wave height in a bay, which can be used by Civil Defense authorities for the implementation of an adequate level of evacuation.

5. Conclusions

[24] On the basis of a pre-computed dataset of 260 scenarios, we developed a robust and reliable forecasting tool to estimate tsunami amplitudes both on the high seas and in targeted coastal areas in French Polynesia. Our method

requires only estimates of epicentral location and seismic moment, and takes about one minute of computing time to run. The tests performed on the four recent Pacific tsunamis with an adequate DART dataset indicate that the agreement between forecast and observed amplitudes deteriorates only at benign amplitudes – on the order of a few cm both on the high seas and in the Polynesian harbors. The systematic overprediction of the 2007 Kuril outer rise earthquake, known to be a violator of scaling laws, suggests that, conversely, tsunami earthquakes would be underpredicted, and that the early observation of this misfit early on into the propagation of the tsunami, could help their identification and thus be beneficial to warning in the far field.

[25] The main limitation of our method is that its application to a given coastal area, such as the Polynesian harbors of Papeete and Taiohae described here, requires a large database of previous observations, in order to define the empirical parameters h_2 , h_E and β used in equation (6). In addition, a “MEGA”-sized event could conceivably straddle partially two of our MEGA sources (e.g., Kuril and Kamchatka), resulting in a lobe of radiation pointed differently in the far field. This situation can be remedied in the future by involving a greater number of overlapping MEGA sources.

[26] **Acknowledgments.** We thank S. Weinstein for a constructive review. Some figures were prepared using GMT software [Wessel and Smith, 1991]. This work was partially supported by ANR (France), under contract 08-RISKMAT-005-01.

[27] The Editor thanks two anonymous reviewers for assisting in the evaluation of this paper.

References

- Ben-Menahem, A., and M. Rosenman (1972), Amplitude patterns tsunami of waves from submarine earthquakes, *J. Geophys. Res.*, *77*, 3097–3128.
- Bilek, S., and T. Lay (1999), Rigidity variations with depth along interplate megathrust faults in subduction zones, *Nature*, *400*, 443–446.
- Courant, R., K. Friedrichs, and H. Lewy (1928), Über die partiellen Differenzgleichungen der mathematischen Physik, *Math. Ann.*, *100*, 32–74.
- Fukao, Y. (1979), Tsunami earthquakes and subduction processes near deep-sea trenches, *J. Geophys. Res.*, *84*, 2303–2314.
- Geller, R. J. (1976), Scaling relations for earthquake source parameters and magnitudes, *Bull. Seismol. Soc. Am.*, *66*, 1501–1523.
- Hayashi, Y. (2010), Empirical relationship of tsunami height between offshore and coastal stations, *Earth Planets Space*, *62*, 269–275.
- Hébert, H., P. Heinrich, F. Schindelé, and A. Piatanasi (2001), Far field simulations of tsunami propagation in the Pacific Ocean: Impact on the Marquesas Islands (French Polynesia), *J. Geophys. Res.*, *106*(C5), 9161–9177.
- Hébert, H., D. Reymond, Y. Krien, J. Vergoz, F. Schindelé, J. Roger, and A. Loevenbruck (2009a), The 18 August 2007 Peru earthquake and tsunami: Influence of the source characteristics on the tsunami height, *Pure Appl. Geophys.*, *166*(1–2), 211–232.
- Hébert, H., D. Reymond, and E. Okal (2009b), Towards a simple quantification of far-field tsunami amplitudes from parameters of the seismic source, *Eos Trans. AGU*, *90*(53), Fall Meet. Suppl., Abstract OS32A-03.
- Kanamori, H. (1972), Mechanism of tsunami earthquakes, *Phys. Earth Planet. Inter.*, *6*, 246–259.
- Kanamori, H., and D. L. Anderson (1975), Theoretical basis of some empirical relations in seismology, *Bull. Seismol. Soc. Am.*, *65*, 587–598.
- Newman, A., and E. Okal (1998), Teleseismic estimates of radiated seismic energy: The E/M_0 discriminant for tsunami earthquakes, *J. Geophys. Res.*, *103*, 26,885–26,898.
- Okada, Y. (1985), Surface deformation due to shear and tensile faults in a half-space, *Bull. Seismol. Soc. Am.*, *75*, 1135–1154.
- Okal, E. A. (1988), Seismic parameters controlling far-field tsunami amplitudes: A review, *Nat. Hazards*, *1*, 67–96.
- Okal, E. A., P.-J. Alasset, O. Hyvernaud, and F. Schindelé (2003), The deficient T waves of tsunami earthquakes, *Geophys. J. Int.*, *152*, 416–432.
- Okal, E., et al. (2010), Field survey of the Samoa tsunami of 29 September 2009, *Seismol. Res. Lett.*, *81*, 577–591.
- Pritchard, M. E., M. Simons, P. Rosen, S. Hensley, and F. Webb (2002), Co-seismic slip from the 1995 July 30 $M_w = 8.1$ Antofagasta, Chile earthquake as constrained by INSAR and GPS observations, *Geophys. J. Int.*, *150*, 362–376.
- Scholz, C. H. (1982), Scaling laws for large earthquakes: Consequences for physical models, *Bull. Seismol. Soc. Am.*, *72*, 1–14.
- Reymond, D., O. Hyvernaud, and E. A. Okal (2012), The 2010 and 2011 tsunamis in French Polynesia: Operational aspects and field surveys, *Pure Appl. Geophys.*, in press.
- Talandier, J., and E. Okal (1991), Single-station estimates of the seismic moment of the 1960 Chilean and 1964 Alaskan earthquakes, using the mantle magnitude M_m , *Pure Appl. Geophys.*, *136*, 103–126.
- Tang, L., V. Titov, and C. Chamberlin (2010), PMEL tsunami forecast series: Vol. 1, A tsunami forecast for Hilo Hawaii, technical report, Pac. Mar. Environ. Lab., NOAA, Seattle, Wash.
- Titov, V., F. González, E. Bernard, M. Eble, H. Mofjeld, J. Newman, and A. Venturato (2005), Real-time tsunami forecasting: Challenges and solutions, *Nat. Hazards*, *35*, 35–41.
- Wessel, P., and W. H. F. Smith (1991), Free software helps map and display data, *Eos Trans. AGU*, *72*, 441.